Journal of Sound and Vibration (2000) **230**(2), 291–308
doi:10.1006/jsvi.1999.2619, available online at http://www.idealibrary.com on IDEAL®

AN ANALYTICAL APPROACH FOR OBTAINING THE LOCATION AND DEPTH OF AN ALL-OVER PART-THROUGH CRACK ON EXTERNALLY IN-PLANE LOADED RECTANGULAR PLATE USING VIBRATION ANALYSIS

S. E. KHADEM AND M. REZAEE

Mechanical Engineering Department, Tarbiat Modarres University, P.O. Box 14155-4838, *Tehran, Iran*

(*Received* 30 *April* 1998, *and in final form* 19 *July* 1999)

In this paper, an analytical approach to the crack detection of rectangular plates under uniform external loades by vibration analysis is established. The damage is considered as an all-over part-through crack parallel to one edge of the plate. Avoiding non-linearity, it is assumed that the crack, at all dynamical conditions, is open. In addition, it is assumed that the plate is simply supported at the two parallel sides, and it has arbitrary boundary conditions at the two other edges. The presence of an all-over part-through crack on the plate introduces considerable local flexibility at the location of the crack. This flexibility is modelled by the stress-intensity factor and compliance. Consideration of important parameters, like, location and depth of an all-over part-through crack, geometry and boundary conditions, magnitude of the external loades, and plate mechanical characteristics on the change of natural frequencies of the cracked plate are the first step for establishing the damage detection method. Vibration analysis of the cracked plate with an all-over part-through crack results in an eigenvalue problem, for which, the solution method is established and is carried out. The solution results are presented by the appropriate charts.

1. INTRODUCTION

Damage detection of one-dimensional structures by vibration analysis, is a new technique in non-destructive evaluation methods. The conventional non-destructive testing methods unlike the vibration analysis methods are expensive and time-consuming. Several researchers have worked on the influence of cracks on the natural frequencies and mode shapes of structures.

Anifantis *et al.* [1] have derived a method for crack detection of beams by vibration analysis. The crack on the beam has been modelled as a local flexibility. The among of flexibility depends on the crack shape and orientation and is computed by fracture mechanics methods. Dias *et al.* [2] have investigated the vibrational behavior of cracked shafts subjected to torsional loads. The crack on the shaft has been modelled as a mode III crack. Moshrefi *et al.* [3] proposed

0022-460X/00/070291 + 18 $35.00/0

a method for determination of a peripheral crack in a thick-walled pipe. The damaged pipe has been modelled as two undamaged beams connected by a hinge and a torsional spring at the crack location.

Because of the complexity of the approach, vibration analysis has been mainly used to study the special cases of vibrational behavior of cracked plates with no emphasis on crack detection. For instance, Lee [4] has used Rayleigh's method with a simple sub-sectioning technique to obtain fundamental frequencies of annular plates with internal concentric cracks. Lee and Lim [5] have investigated the vibrational behaviour of a rectangular plate with a centrally located crack. They have also used Rayleigh's method for determining the natural frequencies of the cracked plate considering the effects of transverse shear deformations and rotary inertia.

The main purpose of the present work is to establish an analytical method for predicting the location and depth of an all-over part-through crack in an externally in-plane loaded rectangular plate using vibration analysis. To this end, one needs natural frequency ratios of the cracked plate to the uncracked one in at least two different vibrational modes, which can be obtained from the experimental modal analysis.

2. MODELLING THE ELASTIC BEHAVIOR OF PLATES WITH AN ALL-OVER PART-THROUGH CRACK SUBJECTED TO A BENDING MOMENT AND AN AXIAL LOAD

Consider an edge-cracked elastic strip with a unit width in the x_1 direction subjected to an axial force N_t and a bending moment M_b as shown in Figure 1. The stress intensity factor (K) of such a loaded cracked strip is given by [6]:

$$K = H^{1/2}(\sigma_t g_t + \sigma_b g_b), \tag{1}$$

where H is the strip thickness, σ_b and σ_t are the nominal stresses at a point away from the crack due to bending moment and axial force effects, respectively ($\sigma_b = 6M_b/H^2$, $\sigma_t = N_t/H$), g_b and g_t are dimensionless functions of the ratio of crack depth to thickness which are given by Gross and Srawley [7] as

$$g_b = \xi^{1/2}(1{\cdot}99 - 2{\cdot}47\xi + 12{\cdot}97\xi^2 - 23{\cdot}11\xi^3 + 24{\cdot}80\xi^4), \tag{2a}$$

$$g_t = \xi^{1/2}(1{\cdot}99 - 0{\cdot}41\xi + 18{\cdot}7\xi^2 - 38{\cdot}48\xi^3 + 53{\cdot}85\xi^4), \tag{2b}$$

where $\xi \equiv h/H$ is the ratio of crack depth to strip thickness. Equations (2a) and (2b) are valid for the range of $0 < \xi < 0{\cdot}7$.

One may consider two identical elastic strips, one of which has an edge crack as shown in Figure 1. If both strips are subjected to a loading system as shown in Figure 1, then the presence of the crack will cause the rotation of one end relative to the other to increase more than the rotation of an uncracked strip, and also the

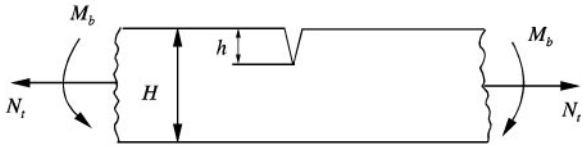

Figure 1. Edge cracked strip.

elongation of the cracked strip will increase. To determine additional rotation of the cracked strip, one may write the relation between the stress intensity factor (K) and potential energy release rate (G), in a state of plane strain, as [8]

$$G = \frac{(1 - \nu^2)}{E} K^2. \tag{3}$$

Upon substitution of the value of K from equation (1) into equation (3), one gets

$$G = \frac{(1 - \nu^2)H}{E} [g_t^2 \sigma_t^2 + \sigma_b^2 g_b^2 + 2 g_b g_t \sigma_b \sigma_t]. \tag{4}$$

On the other hand, one can write G as the sum of potential energy release rates due to bending moment and axial force [6]:

$$G = G_t + G_b = \frac{1}{2}\left[\sigma_t \frac{\partial}{\partial h}(H\delta) + \sigma_b \frac{\partial}{\partial h}\left(\frac{\Theta H^2}{6}\right)\right], \tag{5}$$

where the δ and Θ are the additional stretch and rotation due to the presence of the crack. By comparing equations (4) and (5), one can obtain the additional rotation, Θ, as [6]

$$\Theta = \frac{12(1 - \nu^2)}{E} (\alpha_{bt} \sigma_t + \alpha_{bb} \sigma_b), \tag{6}$$

where the new non-dimensional compliance coefficients α_{bt} and α_{bb} may be computed from the following equations:

$$\alpha_{bb} = \frac{1}{H} \int_0^h g_b^2 \, \mathrm{d}h, \tag{7a}$$

$$\alpha_{bt} = \frac{1}{H} \int_0^h g_b g_t \, \mathrm{d}h. \tag{7b}$$

The values of α_{bb} and α_{bt} depend on the crack depth and strip thickness. As an approximation, one may assume that the stress intensity factor at a point along the

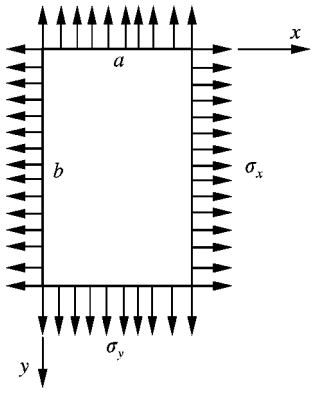

Figure 2. Rectangular plate under external in-plane loads.

crack front of a plate with an all-over part-through constant depth crack, is identical to the stress intensity factor for an edge-cracked strip in plane-strain state with the same loading conditions and crack depth [6].

3. VIBRATION ANALYSIS OF A RECTANGULAR PLATE WITH AN ALL-OVER PART-THROUGH CRACK SUBJECTED TO THE EXTERNAL IN-PLANE LOADS

Consider an elastic rectangular plate with a thickness H and dimensions a and b in x and y directions, as in Figure 2.

If the plate at the boundaries is subjected to uniform distributed external in-plane loads per unit length N_x and N_y, one may derive the governing equation of motion for the free vibration of the plate as [9]

$$\frac{\partial^4 w(x, y, t)}{\partial x^4} + 2\frac{\partial^4 w(x, y, t)}{\partial x^2 \partial y^2} + \frac{\partial^4 w(x, y, t)}{\partial y^4} + \frac{M}{D}\frac{\partial^2 w(x, y, t)}{\partial t^2} = N_x \frac{\partial^2 w(x, y, t)}{\partial x^2} + N_y \frac{\partial^2 w(x, y, t)}{\partial y^2}, \tag{8}$$

where, M is the mass per unit area of the plate, D is the flexural rigidity and N_x and N_y are the stress resultants due to axial external in-plane loads in the x and y directions, respectively. Assuming a harmonic motion, one may use the separation of variables technique as

$$w(x, y, t) = W(x, y)T(t) \tag{9}$$

which upon substitution of relation (9) into equation (8), one obtains

$$\frac{\mathrm{d}^2 T(t)}{\mathrm{d}t^2} + \omega^2 T(t) = 0, \tag{10}$$

$$\frac{\partial^4 W(x, y)}{\partial x^4} + 2\frac{\partial^4 W(x, y)}{\partial x^2 \partial y^2} + \frac{\partial^4 W(x, y)}{\partial y^4} - \frac{M\omega^2}{D} W(x, y) - \frac{N_x}{D}\frac{\partial^2 W(x, y)}{\partial x^2}$$

$$- \frac{N_y}{D}\frac{\partial^2 W(x, y)}{\partial y^2} = 0. \tag{11}$$

The solution of equation (10) is a harmonic function

$$T(t) = A \sin(\omega t + \alpha), \tag{12}$$

where A and α are constants.

By experience, it is highly advantageous to express equation (11) in dimensionless form. Thus, the dimensionless space variables $\zeta \equiv x/a$ and, $\eta = y/b$ may be introduced. Accordingly, equation (11) becomes

$$\frac{\partial^4 W}{\partial \eta^4} + 2\phi^2 \frac{\partial^4 W}{\partial \zeta^2 \partial \eta^2} + \phi^4 \lambda^4 W - \frac{N_x \phi^2 a^2}{D}\frac{\partial^2 W}{\partial \zeta^2} - \frac{N_y \phi^2 a^2}{D}\frac{\partial^2 W}{\partial \eta^2} = 0, \tag{13}$$

where $\phi \equiv b/a$ is the plate aspect ratio, $\lambda^4 \equiv a^4 \omega^2 M/D$, and W is the non-dimensional function of ζ and η.

If the plate is simply supported at the boundaries $\zeta = 0$ and 1, then the following series solution satisfies equation (13) [10]:

$$W(\zeta, \eta) = \sum_{m=1}^{\infty} Y_m(\eta) \sin(m\pi\zeta), \tag{14}$$

By substituting relation (14) into equation (13), one gets [11]

$$\frac{\mathrm{d}^4 Y_m(\eta)}{\mathrm{d}\eta^4} - \left[2\phi^2 (m\pi)^2 + \frac{N_y a^2 \phi^2}{D}\right]\frac{\mathrm{d}^2 Y_m(\eta)}{\mathrm{d}\eta^2} + \phi^4 \left[(m\pi)^4 + (m\pi)^2 \frac{N_x a^2}{D} - \lambda^4\right]$$

$$Y_m(\eta) = 0. \tag{15}$$

To express the solution in a simple form, the following terms are defined:

$$\mathrm{I} \equiv (m\pi)^2 + \frac{n_y}{2}, \tag{16a}$$

$$\mathrm{II} \equiv \left[\left(\frac{n_y}{2}\right)^2 + (m\pi)^2 (n_y - n_x) + \lambda^4\right]^{1/2}, \tag{16b}$$

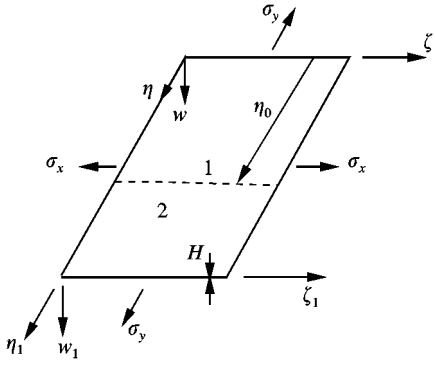

Figure 3. A rectangular in-plane loaded plate with an all-over part-through crack in non-dimensional co-ordinates.

$$n_x \equiv \frac{a^2 N_x}{D}, \tag{16c}$$

$$n_y \equiv \frac{a^2 N_y}{D}, \tag{16d}$$

where n_x and n_y are the dimensionless parameters proportional to stress resultants N_x and N_y. Then the solution of equation (15) for two cases of II > I and II < I, respectively, will be [11]:

$$Y_m(\eta) = A_m \cosh \bar{\beta}_m \eta + B_m \sinh \bar{\beta}_m \eta + C_m \sin \bar{\gamma}_m \eta + D_m \cos \bar{\gamma}_m \eta \tag{17a}$$

$$Y_m(\eta) = A_m \cosh \bar{\beta}_m \eta + B_m \sinh \bar{\beta}_m \eta + C_m \sinh \bar{\gamma}_m \eta + D_m \cosh \bar{\gamma}_m \eta, \tag{17b}$$

where $\bar{\beta}_m = \phi\sqrt{\mathrm{I} + \mathrm{II}}$ and $\bar{\gamma}_m = \phi\sqrt{\mathrm{I} - \mathrm{II}}$ whichever is real.

Now consider a plate containing an all-over part-through crack located at $\eta = \eta_0$ in ζ direction and subjected to external stresses σ_x and σ_y as shown in Figure 3. The plate is divided by the crack in two regions and vibrates as a whole system.

In Figure 3 the new co-ordinates ζ_1, η_1 and W_1 are related to the old co-ordinates ζ, η and W by the following relations:

$$\zeta_1 = \zeta,$$

$$\eta_1 = (\eta - 1), \tag{18}$$

$$W_1 = W.$$

In order to perform the vibration analysis of the cracked plate, one may consider two different types of boundary conditions, (S–S–S–S) and (S–S–S–C).

3.1. SIMPLY SUPPORTED CRACKED PLATE; (S–S–S–S)

In this case, at the crack line (inner boundary) four boundary conditions are defined, and to each external boundary, two boundary conditions are applied. However, because of the form of solutions, the boundary conditions at $\zeta = 0$ and 1 are automatically satisfied. Then, in order to obtain the mode shapes of two regions, one needs only eight boundary conditions. Four of the boundary conditions are applied at the boundaries $\eta = 0$ and $\eta_1 = 0$, and the remaining four are applied to the inner boundaries, where the crack is located, $\eta = \eta_0$. One may note that the elastic behavior of the crack has been used in defining the inner boundary conditions.

Considering Figure 3, and applying the transformation relation (18), the mode shape functions at the η direction for regions (1) and (2) are obtained as [11]

$$Y_{1m} = A_{1m} \cosh \bar{\beta}_m \eta + B_{1m} \sinh \bar{\beta}_m \eta + C_{1m} \sin \bar{\gamma}_m \eta + D_{1m} \cos \gamma \eta_m, \quad (19a)$$

$$Y_{2m} = A_{2m} \cosh \bar{\beta}_m(\eta - 1) + B_{2m} \sinh \bar{\beta}_m(\eta - 1) + C_{2m} \sin \bar{\gamma}_m(\eta - 1)$$

$$+ D_{2m} \cos \bar{\gamma}_m(\eta - 1), \quad (19b)$$

Equations (19a) and (19b) are written for the case of II > I. Similarly, for the case of II < I one may obtain another pair of solutions. The applicable boundary conditions at $\eta = 0$ and $\eta = 1$ are

$$Y_{1m}(0) = Y''_{1m}(0) = Y_{2m}(1) = Y''_{2m}(1) = 0. \quad (20)$$

One can also write inner boundary conditions at the crack location as follows:

$$W_{1\eta} = W_{2\eta}|_{\eta=\eta_0} \text{ (i)}, \; M_{1\eta} = M_{2\eta}|_{\eta=\eta_0} \text{ (ii)}, \; V_{1\eta} = V_{2\eta}|_{\eta=\eta_0} \text{ (iii)} \quad (21)$$

The above equations show the equality of deflections, bending moments and shear forces at the two sides of the crack location respectively. In order to obtain the relation between the rotations of two sides of the crack, one may express σ_t in term of n_y as [11]

$$\sigma_t = \frac{EH^2 n_y}{12(1 - v^2)a^2} \quad (22)$$

and σ_b in terms of lateral deflection of the plate as [12]

$$\sigma_b = \frac{-EH}{2(1 - v^2)} \left(\frac{\partial^2 w}{\partial y^2} + v \frac{\partial^2 w}{\partial x^2} \right). \quad (23)$$

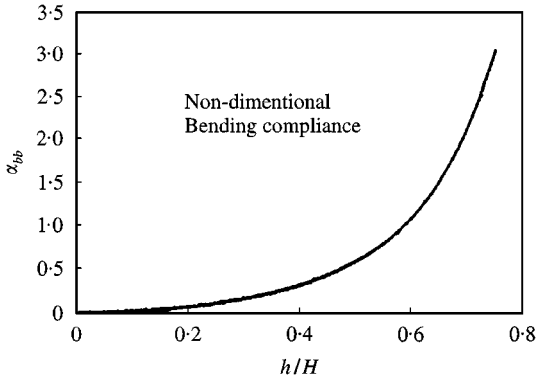

Figure 4. The variation of the dimensionless bending compliance coefficient, α_{bb}, versus relative crack depth $\xi = h/H$ [6].

Upon substitution of equations (22) and (23) into equation (6), one obtains

$$\Theta = \frac{H^2 n_y}{a^2}\alpha_{bt} - 6H\alpha_{bb}\left(\frac{\partial^2 w}{\partial y^2} + v\frac{\partial^2 w}{\partial x^2}\right). \tag{24}$$

In the above relation, the first term is a constant and independent of w, while the second term determines the crack flexibility. One may write the second term in a dimensionless form as, θ:

$$\theta \equiv -\frac{6H}{b}\alpha_{bb}\left(\frac{\partial^2 w}{\partial \eta^2} + v\phi^2\frac{\partial^2 w}{\partial \zeta^2}\right). \tag{25}$$

Then, the fourth inner boundary condition becomes [11]

$$\frac{\partial w_1}{\partial \eta} + \frac{6H}{b}\alpha_{bb}\left(\frac{\partial^2 w_1}{\partial \eta^2} + v\phi^2\frac{\partial^2 w_1}{\partial \zeta^2}\right) - \left.\frac{\partial w_2}{\partial \eta}\right|_{\eta=\eta_0} = 0. \tag{26}$$

By application of the aforementioned boundary conditions and the crack continuity conditions (inner boundary conditions), one may obtain a set of homogeneous equations for the two cases of II > I and II < I.

Setting the determinant of the coefficient matrix equal to zero, one gets the frequency equation of the cracked plate, for the case of II > I as [11]

where $v^* \equiv (2 - v)$.

$$\begin{vmatrix} \sinh \bar{\beta}_m \eta_0 & \sin \bar{\gamma}_m \eta_0 & -\sinh \bar{\beta}_m(1-\eta_0) & -\sin \bar{\gamma}_m(1-\eta_0) \\ \left[\bar{\beta}_m \cosh \bar{\beta}_m \eta_0 + \right. & \left[\bar{\gamma}_m \cos \bar{\gamma}_m \eta_0 - \right. & \bar{\beta}_m \cosh \bar{\beta}_m(1-\eta_0) & \bar{\gamma}_m \cos \bar{\gamma}_m(1-\eta_0) \\ \left. \frac{6H}{b} \alpha_{bb}(\bar{\beta}_m^2 (m\pi^2) v\phi^2) \sinh \bar{\beta}_m \eta_0 \right] & \left. \frac{6H}{b} \alpha_{bb}(\bar{\gamma}_m^2 + (m\pi^2) v\phi^2) \sinh \bar{\beta}_m \eta_0 \right] & & \\ \sinh \bar{\beta}_m \eta_0 (\bar{\beta}_m - (m\pi^2) v\phi^2) & -(\bar{\gamma}^2{}_m + (m\pi^2) v\phi^2) \sin \bar{\gamma}_m \eta_0 & -(\bar{\beta}_m^2 - (m\pi^2) v\phi^2) \sinh \bar{\beta}_m(1-\eta_0) & (\bar{\gamma}_m^2 + (m\pi^2) v\phi^2) \sin \bar{\gamma}_m(1-\eta_0) \\ \bar{\beta}_m(\bar{\beta}_m^2 - (m\pi^2) v^* \phi^2) \cosh \bar{\beta}_m \eta_0 & -\bar{\gamma}_m(\bar{\gamma}_m^2 + (m\pi^2) v^* \phi^2) \cos \bar{\gamma}_m \eta_0 & \bar{\beta}_m(\bar{\beta}_m^2 - (m\pi^2) v^* \phi^2) \cosh \bar{\beta}_m(1-\eta_0) & -\bar{\gamma}_m[\bar{\gamma}_m^2 + (m\pi^2) v^* \phi^2] \cos \bar{\gamma}_m(1-\eta_0) \end{vmatrix} = 0, \quad (27)$$

Similarly, one may obtain the second frequency equation for the case II < I.

The above determinant, is in terms of four parameters α_{bb}, η_0, $\bar{\beta}_m$, and $\bar{\gamma}_m$. If the external loads are known then, the only parameters to play with in the frequency equations will be α_{bb}, η_0, λ.

Since, α_{bb} is related to h/H through relation (7), and to make the analysis easier, one can obtain the relative crack depth, using the Figure 4.

It is evident from the Figure 4 that α_{bb} increases by increasing the value of the relative crack depth.

In the frequency equation, the parameters crucial to the crack detection are h/H, η_0 and λ. Making use of the frequency equation with an integer value of mode numbers m and n (i.e., $m = 1, n = 1$) and setting λ to any sensible value, based on the eigenvalue of the intact plate as an estimation, one can trace the variation of h/H versus η_0 for the range of $\eta_0 = 0$ to 1. At the same time, the new variable R_λ is introduced as

$$R_\lambda \equiv \frac{\lambda_d}{\lambda_I}, \tag{28}$$

where λ_d is the eigenvalue of the damaged plate and λ_I is the eigenvalue of the intact plate at the same mode. The maximum value of R_λ is equal to one, which corresponds to the undamaged plate. This stems from the fact that the undamaged plate is stiffer than the damaged one. To obtain the eigenvalue of the intact plate, λ_I, one may use the following relation as [11]

$$\lambda_I = \left\{ \left[\left(\frac{n}{\phi} \right)^2 + m^2 \right]^2 \pi^4 + \left[n_y \left(\frac{n}{\phi} \right)^2 + (n_x m^2) \pi^2 \right] \right\}^{1/4}. \tag{29}$$

Having the above procedure repeated for the other values of m and n (i.e., $m = 1$, $n = 2$) one can obtain a chart for determining the crack depth and location, keeping in mind that considering only two modes are sufficient for crack detection. As an example, the following mechanical characteristics and dimensions of the plate are used:

$$E = 200 \text{ Gpa}, \qquad a = 0{\cdot}2m,$$

$$v = 0{\cdot}3, \qquad b = 0{\cdot}3\ m,$$

$$\rho = 7860 \text{ kg/m}^3, \qquad H = 0{\cdot}01 \text{ m}$$

for which Figures 5(a)–5(c), the identification charts, are plotted in the co-ordinate system η_0–ξ for aspect ratio of $\phi = 1{\cdot}5$, different values of R_λ, and given values of external stresses σ_x and σ_y ($\sigma_x = N_x/H$, $\sigma_y = N_y/H$).

Figures 5(a)–5(c) have been plotted for the range of $0 \leqslant \eta_0 \leqslant 0{\cdot}5$ due to the symmetry of R_λ curves about $\eta_0 = 0{\cdot}5$.

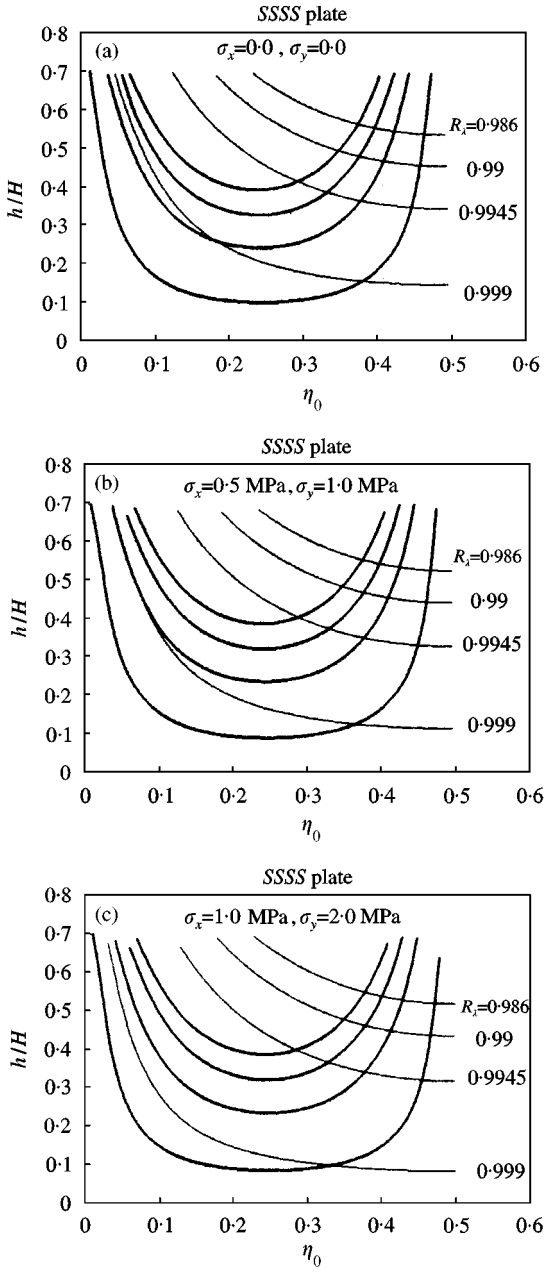

Figure 5. Identification chart for: (a) $\sigma_x = 0$, $\sigma_y = 0$. (b) $\sigma_x = 0{\cdot}5$ MPa, $\sigma_y = 1$ MPa. (c) $\sigma_x = 1$ MPa, $\sigma_y = 2$ MPa.

In Figures 5(a)–5(c), the "U" shape curves correspond to the second vibration mode ($m = 1$, $n = 2$) and the rest of the curves corresponds to the first vibration mode ($m = 1$, $n = 1$). Knowing the external loads and eigenvalue ratios for the first two vibration modes, R_λ, one may construct the identification chart and determine the intersection point of R_λ curves.

The abscissa and the ordinate of the intersection point represent the relative crack location, η_0, and the relative crack depth, ξ respectively. Accordingly, the

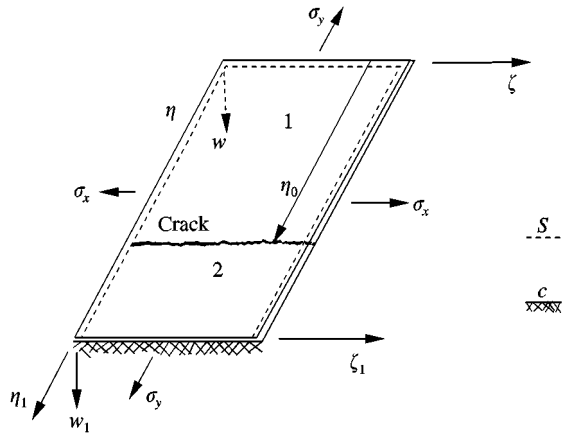

Figure 6. A rectangular cracked plate with (S–S–S–C) edge conditions under external in-plane loads in non-dimensional co-ordinates.

crack depth and location can be obtained from the relations $h = H\xi$, $y = b\eta_0$. In practice, one needs to measure the frequency of the damaged plate using the experimental modal analysis method. Therefore, one may introduce the new definition as "frequency ratio".

$$R_f = \frac{\omega_d}{\omega_I} \tag{30}$$

where ω_d is the natural frequency of the damaged plate at any vibration mode and ω_I is the natural frequency of the intact plate at the same vibration mode. The relationship between the eigenvalue ratio, R_λ, and the frequency ratio, R_f is [11]

$$R_\lambda = R_f^{1/2}. \tag{31}$$

As mentioned before, using the simply supports for all edges of the plate, led to the symmetry of the identification charts, and two solutions were obtained which suggest two different locations for the presence of the crack. This matter obscures the decision making. Therefore, one can remove this deficiency by using different types of supports at $\eta = 0$ and 1 for the crack detection purposes.

3.2. CRACKED PLATE WITH (S–S–S–C) EDGE CONDITIONS

Consider a cracked plate with (S–S–S–C) edge conditions and subjected to a loading system as shown in Figure 6.

To obtain the frequency equation of the uncracked plate, one needs to go to intensive computational efforts, in order to obtain the frequency equation for the intact plate as [11]

$$\bar{\gamma}_m \sinh \bar{\beta}_m^2 \cos \bar{\gamma}_m - \bar{\beta}_m \cosh \bar{\beta}_m \sin \gamma_m = 0. \tag{32}$$

The same procedure is followed to obtain the frequency equation of the cracked plate for the case of II > I [11]:

$$
\begin{vmatrix}
\sinh \bar{\beta}_m\eta_0 & \sin \bar{\gamma}_m\eta_0 & -[\cosh \bar{\beta}_m(\eta_0-1)-\cos \bar{\gamma}_m(\eta_0-1)] & -\left[\sinh \bar{\beta}_m(\eta_0-1)-\dfrac{\bar{\beta}_m}{\bar{\gamma}_m}\sin \bar{\gamma}_m(\eta_0-1)\right] \\
\left\{\bar{\beta}_m \cosh \bar{\beta}_m\eta_0 + \right. & \left\{\bar{\gamma}_m\cos\bar{\gamma}_m\eta_0 - \right. & -[\bar{\beta}_m \sinh \bar{\beta}_m(\eta_0-1)+\bar{\gamma}_m \sin \bar{\gamma}_m(\eta_0-1)] & -\bar{\beta}_m[\cosh \bar{\beta}_m(\eta_0-1)-\cos \bar{\gamma}_m(\eta_0-1)] \\
\left.\dfrac{6H}{b}\alpha_{bb}[\bar{\beta}_m^2-\nu\phi^2(m\pi)^2]\sinh\bar{\beta}_m\eta_0\right\} & \left.\dfrac{6H}{b}\alpha_{bb}[\bar{\gamma}_m^2+\nu\phi^2(m\pi)^2]\sin \bar{\gamma}_m\eta_0\right\} & & \\
[\bar{\beta}_m^2-\nu\phi^2(m\pi)^2]\sinh \bar{\beta}_m\eta_0 & -[\bar{\gamma}_m^2+\nu\phi^2(m\pi)^2\sin \bar{\gamma}_m\eta_0] & \{-[(\bar{\beta}_m^2-\nu\phi^2(m\pi)^2\cosh \bar{\beta}_m(\eta_0-1)] & \left\{-[\bar{\beta}_m^2-\nu\phi^2(m\pi)^2]\sinh \bar{\beta}_m(\eta_0-1)\right. \\
 & & +[\bar{\gamma}_m^2+\nu\phi^2(m\pi)^2\cos \bar{\gamma}_m(\eta_0-1)]\} & \left.+\left[\bar{\beta}_m\bar{\gamma}_m+\nu\phi^2(m\pi)^2\dfrac{\bar{\beta}_m}{\bar{\gamma}_m}\right]\sin \bar{\gamma}_m(\eta_0-1)\right\} \\
\bar{\beta}_m[\bar{\beta}_m^2-\nu\phi^2(m\pi)^2]\cosh \bar{\beta}_m\eta_0 & -\bar{\gamma}_m[\bar{\gamma}_m^2+\nu^*\phi^2(m\pi)^2]\cos \bar{\gamma}_m\eta_0 & -\bar{\beta}_m[\bar{\beta}_m^2-\nu^*\phi^2(m\pi)^2]\sinh \bar{\beta}_m(\eta_0-1) & -\bar{\beta}_m[\bar{\beta}_m^2-\nu^*\phi^2(m\pi)^2]\cosh \bar{\beta}_m(\eta_0-1) \\
 & & -\{\bar{\gamma}_m[\bar{\gamma}_m^2+\nu\phi^2(m\pi)^2]\sin \bar{\gamma}_m(\eta_0-1)\} & +\{\bar{\beta}_m[\bar{\beta}_m^2+\nu^*\phi^2(m\pi)^2]\cos \bar{\gamma}_m(\eta_0-1)\}
\end{vmatrix} = 0 \tag{33}
$$

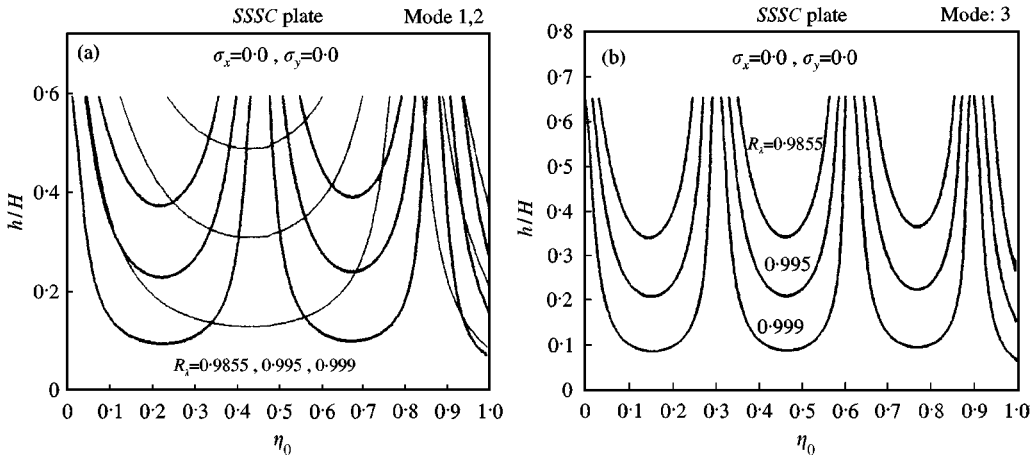

Figure 7. The variation of the relative crack depth (h/H) versus the dimensionless crack location (η_0) for different values of R_λ: (a) for the 1st and 2nd modes, (b) for the 3rd mode.

In fact, using the first two modes will give us more than one intersection point as the crack position. Therefore, one needs to use the third vibration mode to identify exactly the location and depth of the crack. Therefore, there is no symmetry apparent in the Figures 7(a) and 7(b).

3.3. A DISCUSSION ABOUT THE ACCURACY AND THE SENSITIVITY OF THE METHOD

In the present work, for calculating the natural frequencies of the cracked and uncracked plate used for obtaining the relative crack depth and location, the effects of some parameters like, damping, the lack of complete uniformity of the geometrical and mechanical characteristics of the plate, and the lack of true boundary conditions, etc. have been ignored and it is assumed that the geometrical and mechanical characteristics as well as the boundary conditions of the cracked plate are the same as those for uncracked plate. If these assumptions are applicable in practice, the method will work accurately. But due to the aforementioned parameters, the calculated natural frequencies would be the different from those that would have been determined experimentally, causing some errors in the method.

To analyze the accuracy and the sensitivity of the approach to errors and inaccuracies, consider a crack at a relative location $\eta_0 = 0{\cdot}4$, and check the effect of the relative crack depth by having $h/H = 0{\cdot}2$ and $h/H = 0{\cdot}6$.

For the case of $h/H = 0{\cdot}2$ and by referring to Figure 5(a), the eigenvalue ratios at the first mode ($m = 1$, $n = 1$) and the second mode ($m = 1$, $n = 2$), can be obtained as

$$R_{\lambda_{11}} = 0{\cdot}9984, \qquad R_{\lambda_{12}} = 0{\cdot}9987$$

using equation (31), the corresponding frequency ratios would be

$$R_{f_{11}} = 0{\cdot}9968, \qquad R_{f_{12}} = 0{\cdot}9974.$$

By referring to the mechanical and geometrical characteristics used for the curves in Figure 5(a), the decrease of natural frequencies of the plate due to the presence of a crack with $h/H = 0{\cdot}2$, at the above-mentioned modes can be obtained as

$$\Delta_{f_{11}} = 2{\cdot}77 \text{ Hz}, \qquad \Delta_{f_{12}} = 4{\cdot}33 \text{ Hz}.$$

If the last calculations are repeated for the case of $h/H = 0{\cdot}6$, the following results will be obtained:

$$R_{\lambda_{11}} = 0{\cdot}9840, \quad R_{f_{11}} = 0{\cdot}9683, \quad \Delta_{f_{11}} = 27{\cdot}45 \text{ Hz},$$

$$R_{\lambda_{12}} = 0{\cdot}9870, \quad R_{f_{12}} = 0{\cdot}9742, \quad \Delta_{f_{12}} = 42{\cdot}96 \text{ Hz}.$$

By considering an error equal to 0·2% in calculating the frequency ratios, the maximum and minimum values of frequency ratios, eigenvalue ratios, as well as the maximum and minimum values of reduction in natural frequencies for the case of $h/H = 0{\cdot}2$ will be as follows:

$$(R_{f_{11}})_{\max} = 0{\cdot}9988, \qquad (R_{\lambda_{11}})_{\max} = 0{\cdot}9994, \quad (\Delta_{f_{11}})_{\max} = 2{\cdot}78 \text{ Hz},$$

$$(R_{f_{11}})_{\min} = 0{\cdot}9948, \qquad (R_{\lambda_{11}})_{\min} = 0{\cdot}9974, \quad (\Delta_{f_{11}})_{\min} = 2{\cdot}76 \text{ Hz},$$

$$(R_{f_{12}})_{\max} = 0{\cdot}9994, \qquad (R_{\lambda_{12}})_{\max} = 0{\cdot}9997, \quad (\Delta_{f_{12}})_{\max} = 4{\cdot}34 \text{ Hz},$$

$$(R_{f_{12}})_{\min} = 0{\cdot}9954, \qquad (R_{\lambda_{12}})_{\min} = 0{\cdot}9977, \quad (\Delta_{f_{12}})_{\min} = 4{\cdot}32 \text{ Hz}$$

and for the case of $h/H = 0{\cdot}6$, one can obtain

$$(R_{f_{11}})_{\max} = 0{\cdot}9702, \qquad (R_{\lambda_{11}})_{\max} = 0{\cdot}9850, \qquad (\Delta_{f_{11}})_{\max} = 27{\cdot}50 \text{ Hz},$$

$$(R_{f_{11}})_{\min} = 0{\cdot}9664, \qquad (R_{\lambda_{11}})_{\min} = 0{\cdot}9830, \qquad (\Delta_{f_{11}})_{\min} = 27{\cdot}40 \text{ Hz},$$

$$(R_{f_{12}})_{\max} = 0{\cdot}9761, \qquad (R_{\lambda_{12}})_{\max} = 0{\cdot}9880, \qquad (\Delta_{f_{12}})_{\max} = 43{\cdot}05 \text{ Hz},$$

$$(R_{f_{12}})_{\min} = 0{\cdot}9723, \qquad (R_{\lambda_{12}})_{\min} = 0{\cdot}9860, \qquad (\Delta_{f_{12}})_{\min} = 42{\cdot}87 \text{ Hz}.$$

Now, if curves, same as those in Figure 5(a) are plotted by interpolation for values of $(R_{\lambda_{11}})_{\max}$, $(R_{\lambda_{11}})_{\min}$, $(R_{\lambda_{11}})_{\max}$ and $(R_{\lambda_{12}})_{\min}$ corresponding to the case of $h/H = 0{\cdot}2$, the enclosed area among these curves will be a geometric locus for possible answers of relative crack depth and location. In the mentioned area, the

values of h/H and η_0 vary from 0·12 to 0·25 and 0·33 to 0·46 respectively. In other words, an error equal to 0·2% in calculating the frequency ratios causes maximum errors in obtaining the relative crack depth and location equal to $\pm 0{\cdot}8$ and $\pm 0{\cdot}7$ respectively.

By considering the above analysis for the case of $h/H = 0{\cdot}6$, the values of h/H and η_0 vary from 0·57 to 0·62 and 0·38 to 0·42 respectively. In this case the maximum errors in obtaining the relative crack depth and location will be $\pm 0{\cdot}03$ and $\pm 0{\cdot}02$ respectively.

As a result, the proposed method for obtaining the crack depth and location is sensitive to the errors; for a certain value of the error in obtaining the frequency ratio, by increasing the depth of the crack the enclosed area among the curves will be reduced. So the influence of errors on obtaining the crack depth and location, will be reduced. However, by decreasing the depth of the crack, the area of the geometric locus for possible solutions will increase; thus, the accuracy of the method will be reduced.

In addition, by comparing the calculated Δ_fs in the above example, it is obvious that, for a certain relative crack location, the less the depth of the crack, the less the natural frequencies of the cracked plate will be reduced. Therefore, the value of the error resulting from inaccuracies of measurements will be increased, while for deeper cracks, the reduction of the natural frequencies of the cracked plate is considerable and the errors in comparison with those values will be insignificant.

Furthermore, it should be noted that while the R_λ values are close to unity and the differences between them are so small, the corresponding differences between the natural frequencies of uncracked and cracked plate (Δ_f) are significant.

4. CONCLUSIONS

Introduction of an all-over part-through crack in a plate subjected to external loads decreases the natural frequencies of the plate and by growing the crack depth, the growth rate of the local flexibility is accelerated. By increasing the crack depth, the natural frequencies diminish. On the other hand, presence of a crack with special depth, depending on its location, would affect each of the natural frequencies differently.

In the case of simply supported plate, as much as the crack becomes close to the boundaries $\eta = 0$ and 1, the influence of the crack on the natural frequencies is reduced and for other regions this effect depends on vibration mode. Other parameters like external loads applied at the boundaries also influence the plate natural frequencies. By comparing Figures 5(a)–5(c) it is apparent that by increasing the external loads, the intersection points of curves are altered, and the trend of these changes at larger values of eigenvalue ratios is quite obvious. Also from these figures, it is clear that on the $\xi = h/H =$ constant line for the first vibration mode, the value of the eigenvalue ratio (R_λ) diminishes by distance away from the boundaries ($\eta = 0$, 1).

This means that, the influence of an all-over part-through crack with a constant depth on the first natural frequency of the cracked plate increases as much as it gets closer to the center of the plate ($\eta_0 = 0{\cdot}5$). The same situation for the second

vibration mode takes place at in the range of $\eta_0 = 0$ and 0·25. In other words, the maximum effect of an all-over part-through crack with a constant depth on the second natural frequency occurs when the crack is located at $\eta_0 = 0{\cdot}25$ or 0·75. In Figures 5(a)–5(c) the value of crack relative depth (ξ) at the boundaries $\eta_0 = 0$ and 1 for any value of R_λ, becomes infinity (from a theoretical stand point), which means that at the first vibration mode ($m = 1$, $n = 1$) of simply supported plate, there is no bending moment at the simply supported edges. In other words, the κ_y (curvature of the mid plane of the plate at y direction) at the simply supported edges is zero. The aforementioned case for the second vibration mode occurs at the three points ($\eta = 0$, 0·5 and 1). At these points, the presence of an all-over part-through crack would not affect the corresponding natural frequencies of the intact plate.

This result cannot be extended to the other type of edge conditions. For instance, if the plate is clamped at $\eta = 1$ (as described at section 3.2), then any deflection due to transverse vibration of the plate causes bending moments at the clamped edge. Therefore, if we use the two different kinds of supports at the boundaries $\eta = 0$ and 1, then the symmetry of the $R_\lambda =$ constant curves with respect to the point $\eta = 0{\cdot}5$ will be removed as shown in Figures 7(a) and 7(b). In this case, one can obtain a single solution by intersecting the $R_\lambda =$ constant curves at three vibration modes. The advantage of this case is that a unique solution is obtained which suggests the crack location exactly.

REFERENCES

1. N. Anifantis, P. Rizos and A. Dimarogonas 1986 *Advanced Topics in Vibration*, 189–197. Identification of cracks on beams by vibration analysis.
2. J. C. Dias, D. Spinelli and P. Seleghim 1986 *Advanced Topics in Vibration*, 33–36. Analysis of discrete vibration system containing cracked elements.
3. N. Moshrefi, H. A. Sereshta and W. T. Springer 1986 *Advanced Topics in Vibration*, 23–29. The transverse vibrational characteristics of an externally damaged pipe.
4. H. P. Lee 1992 *Computers and Structures* **43**, 1085–1089. Fundamental frequencies of annular plates with internal cracks.
5. H. P. Lee and S. P. Lim 1993 *Computers and Structures* **49**, 715–718. Vibration of cracked rectangular plates including transverse shear deformation and rotary inertia.
6. J. R. Rice and N. Levy 1972 *Journal of Applied Mechanics* **3**, 185–194. The part-through surface crack in an elastic plate.
7. B. Gross and J. E. Srawley 1965 *NASA Technical Note D*.2603. Stress-intensity factor for single edge notch specimens in bending or combined bending and tension by boundary collocation of a stress function.
8. S. A. Meguid 1989 *Engineering Fracture Mechanics*. Amsterdam: Elsevier Science Publishers Ltd.
9. C. M. Harris 1988 *Shock and Vibration Handbook*. McGraw-Hill, third edition.
10. D. J. Gorman 1982 *Free Vibration Analysis of Rectangular Plates*. Amsterdam: Elsevier, North-Holland. Inc.
11. M. Rezaee 1995 *M.Sc. Thesis, Tarbiat Modarres University*. Development and the application of the vibration analysis to the fault detection of plates under the external loads.
12. A. C. Ugural 1981 *Structures in Plates and Shells* New York, McGraw-Hill.

APPENDIX: NOMENCLATURE

a,b	plate dimensions
D	plate flexural rigidity, $= EH^3/12(1-v^2)$
E	Young's modulus
g_b, g_t	dimensionless functions
G, G_b, G_t	potential energy release rate
H	plate thickness
h	crack depth
K	stress intensity factor
M	mass per unit area of the plate
M_b	bending moment
m, n	mode numbers
N_t, N_x, N_y	stress resultants (axial force per unit length)
n_x, n_y	non-dimensional external force
R_f	frequency ratio
R_λ	eigenvalue ratio
$T(t)$	time dependent function
$V_{1\eta}\cdots$	shear force per unit length
W, w	transverse deflection
x, y, z	rectangular co-ordination axis
α_{bb}, α_{bt}	dimensionless compliance coefficients
$\bar{\beta}_m$, $\bar{\gamma}_m$	non-dimensional frequency parameters
ζ, η	dimensionless co-ordinates
Θ, θ	slope discontinuity at crack location
λ_1	eigenvalue of the intact plate
λ_d	eigenvalue of the damaged plate
v	the possion ratio
ξ	relative crack depth
ρ	mass per unit volume of the plate
σ_b	bending stress
σ_t	normal stress due to axial force
ϕ	plate aspect ratio
ω_I	natural frequency of the intact plate
ω_d	natural frequency of the damaged plate
I, II	dimensionless parameters